# Empirical Satellite Spectrum Occupancy Modeling and Testbed in the L-Band

Michael Aygur\*, Sithamparanathan Kandeepan\*, Fernando Moya Caceres\*, Akram Al-Hourani\*,
Bo Li<sup>†</sup>, Sam Reisenfeld<sup>†</sup>, Ediz Cetin<sup>†</sup>, and Mark Bowyer<sup>‡</sup>

\* Department of Electrical and Electronic Engineering, RMIT University, Melbourne, Australia {michael.aygur, kandeepan, fernando.moyacaceres, akram.hourani}@rmit.edu.au

† School of Engineering, Macquarie University, Sydney, NSW, Australia
{bo.li, sam.reisenfeld, ediz.cetin}@mq.edu.au

‡ Airbus Defence & Space, Portsmouth, United Kingdom
mark.bowyer@airbus.com

Abstract-Communication systems such as satellite communication (SATCOM) systems operate in regulated frequency bands and are often separated based on the radio service to control the interference. The satellite-to-earth link can be studied using a software-defined radio (SDR) by capturing and storing the satellite data. This paper aims to create a methodology that can be used to capture and model satellite traffic in a desired frequency band. We cover the testbed setup to capture the satellite signals, the necessary processing steps to extract useful information from the captured data, and the spectrum occupancy modeling. The short-time Fourier transform (STFT) and density-based spatial clustering of applications with noise (DBSCAN) algorithm are used to packetize the captured satellite data. The holding, idle, and inter-arrival times were obtained to determine the occupancy rate and occupancy duration over a one-week period. Using these empirical quantities, satellite packet traffic was generated and compared to the experimental data.

Index Terms—SATCOM, traffic modeling, SDR, DBSCAN, occupancy rate, occupancy duration.

#### I. INTRODUCTION

The SATCOM sector has thrived due to its geographical advantage over terrestrial alternatives, with low-latency satellite broadband services now available for consumer use [1]. The radio frequency (RF) bands for satellite services are regulated by the International Telecommunication Union (ITU) with services including the global position system (GPS) in the L-band, television and radio broadcasting in the S-band, and high-throughput applications in the X and Ku-bands [2]. Satellite traffic in the satellite-to-earth link would therefore be different; dependent on the satellite service application (low vs. high data rate), the operator of the satellite (military vs. commercial), and the sharing of RF resources between the geostationary orbit (GEO) and next-generation low Earth orbit (LEO) satellites [3].

The RF resource is shared by terrestrial and non-terrestrial services but is limited in nature with minimal RF overlap to better manage the interference between services. However, the spectrum can be under-utilized due to end user application requirements (streaming vs. burst), spatial separation, and time of day. To improve spectrum sharing, accurate spectrum occupancy models are required as they can quantify useful traffic characteristics of the service such as the occupancy rate

and occupancy duration. With increased attention in satellite service areas, understanding this spectrum usage can assist in RF coexistence efforts with terrestrial services in the same RF spectrum. Furthermore, dynamic spectrum access (DSA) can utilize such models to facilitate this spectrum sharing.

We measured the satellite activity in western Melbourne, Australia, to produce models for the satellite-to-earth Inmarsat link in the 1540 MHz band. Our key contributions are the framework for experimental satellite channel spectrum occupancy, the testbed development and modeling, and the results that provide knowledge into the spectrum utilization of practical SATCOM links for the given band.

# II. LITERATURE REVIEW

Spectrum management issues licenses or authorizations for spectrum use based on the spectrum monitoring of channel and band usage, which include channel availability statistics to form the spectrum occupancy [4]. Unlike this traditional spectrum management, cognitive radio (CR) and DSA wish to utilize the spectrum more dynamically to improve the spectrum occupancy with minimal additional overhead. The spectrum monitoring information is still used to make informed decisions which has motivated many measurement campaigns globally [5]–[7]. The satellite measurements found in these studies evaluated frequencies in the ultra high frequency (UHF) band (300-3000 MHz) where radionavigation, mobile, broadcasting, and Earth exploration satellite services are present above 1000 MHz as per the ITU frequency allocations. In each case, the satellite bands were considered as one frequency range to simplify the studies where a threshold (energy or power) was used to determine the spectrum occupancy. However, the satellite signal may be too weak for these studies due to the large propagation distance.

The spectrum data was showcased in the frequency domain as it is a good way to observe spectrum occupancy [4] where they used varying thresholds per band [5]. However, the spectrum occupancy is dependent on the threshold value chosen due to false alarms and missed detections [8]. The mean spectrum occupancy per band was usually reported on which may not be suitable for practical CR applications. Furthermore, incorporating the time domain along with the

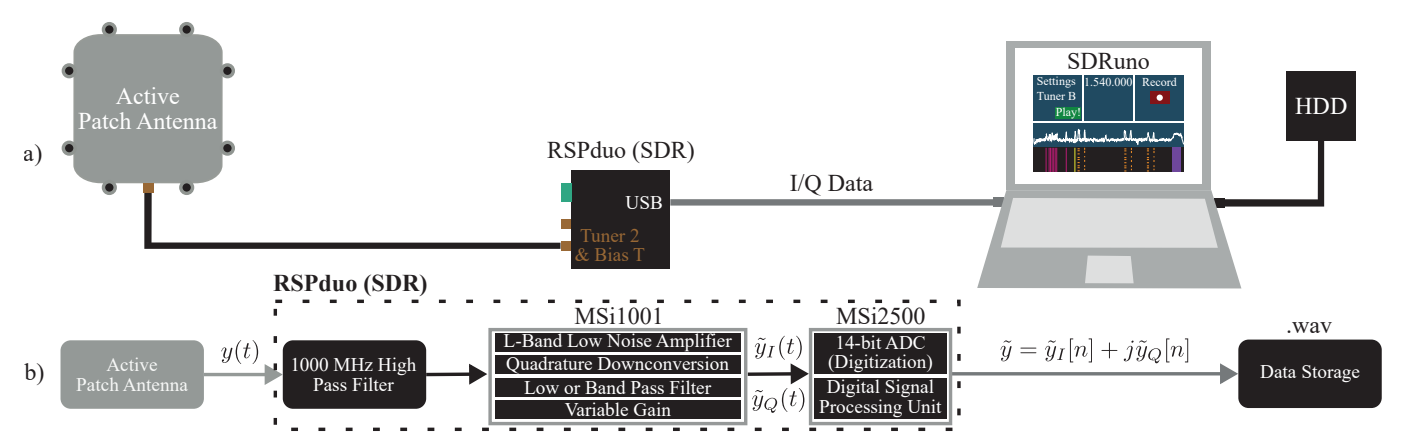


Fig. 1. Testbed architecture for capturing Inmarsat satellite signals in the L-band at 1540 MHz: a) The physical implementation of the testbed using commercial off-the-shelf devices (COTS); b) The spectrum data capturing pipeline.

frequency domain is useful for an analysis over short periods of time [4] which would improve DSA efforts, e.g., the STFT can be used to transform a signal to the time-frequency domain. Lastly, models can be developed from the spectrum management information to assess spectrum sharing by analyzing the probability of interference [4].

# III. SYSTEM MODEL

A range of satellite services operate in the L-band globally such as GPS and the Inmarsat network [2]. In Australia, the Australian Media and Communications Authority (ACMA) hosts a database of frequency licenses that was used to confirm Inmarsat L-band satellite activity<sup>1</sup>. Therefore, satellite traffic can be easily captured using a SDR and antenna.

# A. Experimental Testbed

The testbed architecture for capturing and storing Inmarsat L-band satellite activity is depicted in Fig. 1a. The testbed uses an active L-band patch antenna with an internal low noise amplifier (LNA) to produce a sufficiently high-gain and wide-beamwidth antenna. The antenna, with sufficient elevation, can be positioned perpendicular to the ground or pointed towards the satellite for optimal modeling.

A range of SDRs can be utilized for capturing RF signals, each with varying hardware interfaces and performance. The chosen SDR was the RSPduo by SDRplay due to its good receiver performance at an affordable price and includes an inbuilt bias T to supply power to the active antenna [9]. The RSPduo is connected to a computing device (laptop) via a USB interface for its power supply and data sink.

A computing device controls the RSPduo via the vendor software SDRuno to perform a range of tasks such as monitoring and capturing the spectrum [9]. SDRuno supports 32-bit waveform audio file (WAV) formats to store the uncompressed spectrum data [two 16-bit channels for the in-phase and quadrature (I/Q) signal] to an external hard drive disk (HDD).

# B. Signal Model

The spectrum capturing pipeline is depicted in Fig. 1b. The received RF signal at a center frequency  $f_c$  is given by,

$$y(t) = a(t; f_c) + n(t) \tag{1}$$

where  $a(t;f_c)$  is the received satellite signal at the carrier frequency  $f_c$  and n(t) is the additive white Gaussian noise (AWGN) at the receiver. The RSPduo hardware applies a high pass filter (HPF) to attenuate RF signals below 1000 MHz before a L-band LNA in the range 1450-1675 MHz is applied by the MSi1001 tuner [10]. The MSi1001 tuner then performs the quadrature downconversion to produce the analog in-phase  $\tilde{y}_I(t)$  and quadrature  $\tilde{y}_Q(t)$  components that are filtered. Afterwards, the output is amplified and passed to the MSi2500 14-bit analog-to-digital converter (ADC) and digital signal processing (DSP) unit to produce the digitized samples  $\tilde{y} = \tilde{y}_I[n] + j\tilde{y}_Q[n]$  that are sent to the computing device via USB for post-processing.

# IV. FRAMEWORK FOR EXPERIMENTAL SPECTRUM OCCUPANCY ANALYSIS

We captured the L-band satellite traffic over a one-week period which started on December 14 (Saturday), 2024, and finished on December 20 (Friday), 2024. The Coordinated Universal Time (UTC) was used to initiate the captures and will be referenced to herein. We decided on eight one-hour observation periods to examine the traffic behavior at 1540 MHz over a 1 MHz bandwidth, with the start of each period listed in 24-hour time: i) 00:00, ii) 03:00, iii) 06:00, iv) 09:00, v) 12:00, vi) 15:00, vii) 18:00, and viii) 21:00. Therefore, a total of 56 observation periods will be used for modeling.

The file size for each observation period will be approximately 14.4 GB when using a sampling rate  $f_s$  of 1 MHz. However, SDRuno will create four files per observation period due to the 32-bit WAV format file size limit of 4 GB. The total storage requirement is 806.4 GB which allows us to store all the uncompressed spectrum data to a 1 TB HDD for later processing.

<sup>&</sup>lt;sup>1</sup>The license number 10247442/1 belongs to Inmarsat Solutions B.V (Aerospace) which authorizes communications with INMARSAT-4A 143.5E at a center frequency of 1.5403 GHz and bandwidth of 1000 kHz.

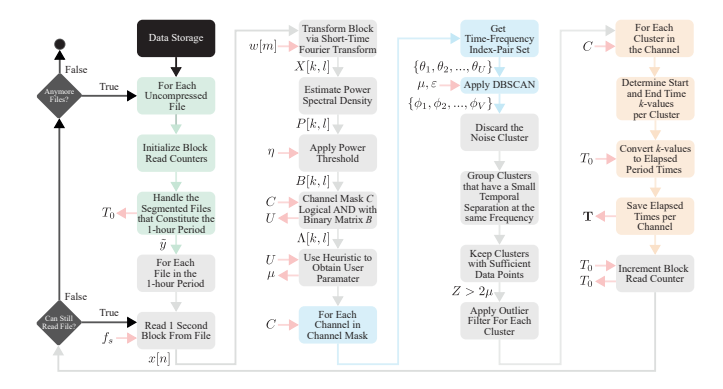


Fig. 2. Data processing flowchart to extract the holding, idle, and inter-arrival times based on the recorded I/Q data that was collected using the testbed.

## A. Data Processing

We have summarized our data processing methodology in Fig. 2 which extracts the key temporal properties of the satellite channels, over all observation periods, from the measurement campaign for later modeling. We utilize MATLAB to execute the data processing steps. We read continuous blocks of  $N_x$  samples from the large set of samples in  $\tilde{y}$ , that is stored in the HDD, to generate the STFT for our analysis where we define this signal block as x[n]. We use a  $N_{DFT}$  point discrete Fourier Transform (DFT) on multiple signal blocks of M time domain samples with a windowing function w[m] where  $1 \leq m \leq M$ , using a hop size of H between DFTs blocks to produce a signal overlap of (M-H) samples for the STFT signal. The window will dictate the time and frequency resolution of the STFT such that narrow windows (small M) will have improved time resolution at the cost of a lower frequency resolution as the DFT is used on less samples, and vice versa. The STFT output of x[n], given by X[k,l], is a  $N_{DFT} \times N_t$  size matrix with  $N_{DFT}$  frequency-rows of width  $\Delta f = f_s/N_{DFT}$  Hz and  $N_t = \lfloor (N_x - (M-H))/(M - (M-H)) \rfloor$  time-columns with length  $\Delta t = N_x/(f_s N_t)$  seconds, where  $1 \le l \le N_{DFT}$ and  $1 \leq k \leq N_t$ . The other STFT parameters were set to  $N_{DFT} = 2048$ ,  $M = |f_s/1024|$  using a Hamming window function, and H = M for zero overlapping samples. We can calculate the normalized power spectral density (PSD) by

$$P[k,l] = \frac{|X[k,l]X^*[k,l]|}{f_s \sum_{m=1}^{M} w[m]^2}$$
 (2)

where  $X^*[k,l]$  is the conjugate of X[k,l]. The total energy for the M-point time domain window samples in w[m] was obtained using Parseval's theorem to scale the PSD. The PSD values are converted to dBm/Hz using  $10\log_{10}(P)$  as we believe that SDRuno scales each I/Q value to mW during I/Q recording. By applying the threshold  $\eta$  to every element in P, we can obtain a binary matrix B which can reveal the spectrum usage in time and frequency as

TABLE I CHANNELS IN THE CHANNEL MASK GIVEN AS FREQUENCY BINS AND FREQUENCY RANGES

Channel Number	Freq. Bin Range (l-values)	Freq. Range (MHz)
c = 1	600-680	1539.79-1539.83
c = 2	680-750	1539.83-1539.87
c = 3	1030-1080	1540.00-1540.03
c = 4	1080-1110	1540.03-1540.04
c = 5	1220-1300	1540.10-1540.13
c = 6	1300-1360	1540.13-1540.16
c = 7	1520-1600	1540.24-1540.28
c = 8	1600-1660	1540.28-1540.31

$$B[k,l] = \begin{cases} P[k,l] \ge \eta, & \text{occupied (1)} \\ P[k,l] < \eta, & \text{background (0)} \end{cases}$$
 (3)

The value of  $\eta$  was 3 dB above the thermal noise power at 30 degree Celsius with the bandwidth equal to  $f_s$  and RSPduo noise figure (NF) of 4.3 dB at 1500 MHz [9], resulting in  $\eta = -106.49$  dBm. The noise power distribution of the testbed could also be used to determine  $\eta$  [8] by recording noise samples under clear sky conditions facing away from the satellite or in a shielded room at the target frequency. Two uncertainty conditions can occur: i) strong noise crossing  $\eta$  which is a false alarm; ii) weak signals falling below  $\eta$  which is a missed detection. To improve B, a trained machine learning agent could be used to better detect the signals [11].

# B. Data Clustering

We follow a similar procedure that is outlined in [8] to form packets from B. We present in Fig. 3 the key steps that were shown in Fig. 2 and further discuss them here. We used a channel mask C as the traffic in this band was observed to have channels unlike the Industrial, Scientific, and Medical (ISM) band as was done in [8]. This can improve the results of the clustering algorithm for close groups, reduce the computational burden of the clustering algorithm due to a reduction of data points, and improve temporal property extraction. C is a  $N_{DFT} \times N_t$  size binary matrix, initialized to all zeroes, with many grouped all-one row-vectors to represent a channel c out of  $N_c$  channels. The observed channels are provided in Table I. We obtain the matrix  $\Lambda = B \wedge C$  by using the logical AND operator element-wise.

The DBSCAN algorithm created the *packets* using only three parameters: i) the data as a set of time-frequency index pairs  $\{\theta_1,\theta_2,...,\theta_U\}$  where  $\theta_u=(k,l):\Lambda[k,l]=1$  is the u-th time-frequency pair out of the total  $U\leq N_{DFT}N_t$  pairs that is above the threshold  $\eta$  to satisfy the condition in (3). ii) The maximum search radius  $\varepsilon$  with  $\varepsilon=4$  being used. iii) The minimum number of required points in the search radius is  $\mu=\lfloor\ln(U)\rfloor$  which is a heuristic [8] that dynamically adjusts the requirements to form a cluster.

With these three parameters, DBSCAN produces the set of clusters  $\{\phi_1,\phi_2,...,\phi_V\}$  where  $\phi_v=\{\theta_1,\theta_2,...,\theta_Z\}:\mu\leq Z\leq U$  is the v-th cluster. DBSCAN also returns the noise cluster which we do not use. The clusters are regrouped if

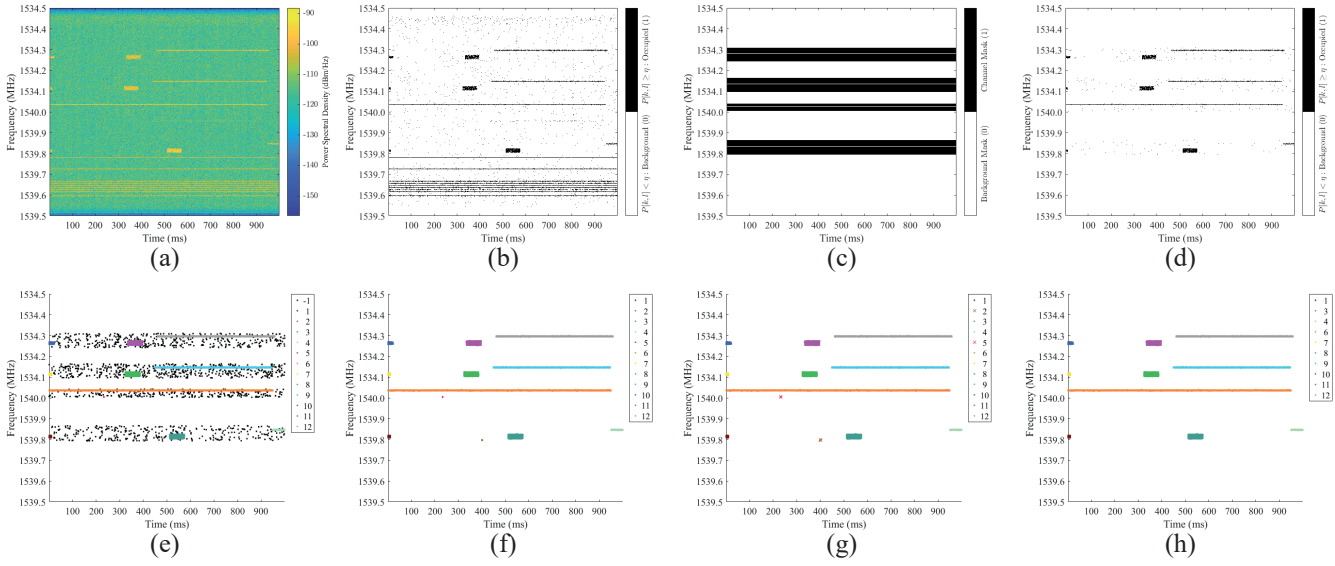


Fig. 3. The data clustering algorithm with the key steps highlighted to model L-band satellite traffic. (a) is the PSD P[k, l] in dBm/Hz given in (2). (b) is the binary matrix B[k, l] given in (3). (c) is the channel mask C. (d) is the logical AND operation between (b) and (c). (e) is the initial output of the DBSCAN algorithm with the noise cluster represented by '-1'. (f) is the output of the DBSCAN algorithm without the noise cluster followed by a regrouping of clusters with small temporal separation in the same channel. (g) is the cluster rejection step to retain significant clusters. (h) is the output of the outlier filter.

a small temporal separation between clusters at the same frequency range was found, which was due to some long (time) but narrow (frequency) signals. We achieve this by determining the start and end time k-values for each cluster (packet). The start time of  $\phi_v$  was found using

$$k_{\rm s} = \min_{k}(\phi_v) = \min_{k}(\{\theta_1, \theta_2, ..., \theta_Z\})$$
 (4)

and the end time of  $\phi_v$  was found using

$$k_{\rm e} = \max_{k}(\phi_v) = \max_{k}(\{\theta_1, \theta_2, ..., \theta_Z\}).$$
 (5)

Clusters are discarded if they do not satisfy  $Z>2\mu$  as they are deemed to be additional noise clusters that formed due to the false alarm uncertainty. Lastly, an outlier filter discards any pairs in a cluster where the time or frequency value was 1.5 points above the upper or below the lower quartile.

# C. Temporal Formatting of Spectral Data

To extract the temporal statistics from these clusters, we used two block read counters to: i) read from the current file in one observation period; ii) keep track of the total block read number across the four files to determine the elapsed time. We use (4) and (5) for each cluster that is contained within each channel. We translate the column indexes to a time value using  $T(k) = k\Delta t + T_0$  where  $T_0$  is the total block read number. The values obtained from this translation, using  $k_{\rm s}$  and  $k_{\rm e}$  for the given channel's cluster, are stored in  $T_c = \left\{ \left\{ T_{\rm s,1}, T_{\rm e,1} \right\}, ..., \left\{ T_{\rm s,N_p}, T_{\rm e,N_p} \right\} \right\}$  where  $T_c$  contains all the start  $(T_{\rm s})$  and end time  $(T_{\rm e})$  values for channel c in one observation period, with a total of  $N_p$  packets identified in c. Both counters are incremented after all channels and

clusters have been processed. The first counter resets to 1 when the next file in the observation period is being read.

Due to the block-by-block read approach undertaken, there is a high possibility of signals being 'split' across one or more reads. We can detect this in the channel's  $\mathbf{T}$  matrix, i.e., we can logically test if the end time of  $packet\ T_{e,p}$  is equal to the start time of the next  $packet\ T_{s,(p+1)}$  in  $\mathbf{T}_c$ . When true,  $T_{e,p}$  is set to  $T_{e,(p+1)}$  with the packet  $\{T_{s,(p+1)},T_{e,(p+1)}\}$  being discarded from  $\mathbf{T}_c$ . Therefore, we apply this process for  $1 \leq p \leq N_p$  for each channel c.

# V. INMARSAT SATELLITE-TO-EARTH SPECTRUM OCCUPANCY MODELING

Recall that eight one-hour observation periods were captured per day over a week. For each observation period, the set  $\{\mathbf{T}_1, \mathbf{T}_2, ..., \mathbf{T}_{N_c}\}$  stores the *packets* for channels  $1 \leq c \leq N_c$  over one period. We use three traffic properties to model the satellite traffic in the 1540 MHz band based on these *packets*, namely the holding, idle, and inter-arrival times. Briefly, A channel can be assumed to be in one of two states: idle or busy. The time spent in the busy state before a transition back to the idle state is the holding time  $(T_{\rm H})$ . Then, the time until the next transition from the idle state to the busy state is the idle time  $(T_{\rm I})$ . Finally, the inter-arrival time  $(T_{\rm IA})$  is the time interval between the start of one busy state to the next busy state. We can apply this notion here using the following:

$$T_{H,p} = T_{e,p} - T_{s,p}$$
 (6)

$$T_{I,p} = T_{s,(p+1)} - T_{e,p}$$
 (7)

$$T_{\text{IA},p} = T_{\text{s},(p+1)} - T_{\text{s},p}$$
 (8)

where  $1 \leq p \leq N_p$  is a packet from  $\mathbf{T}_c$ .

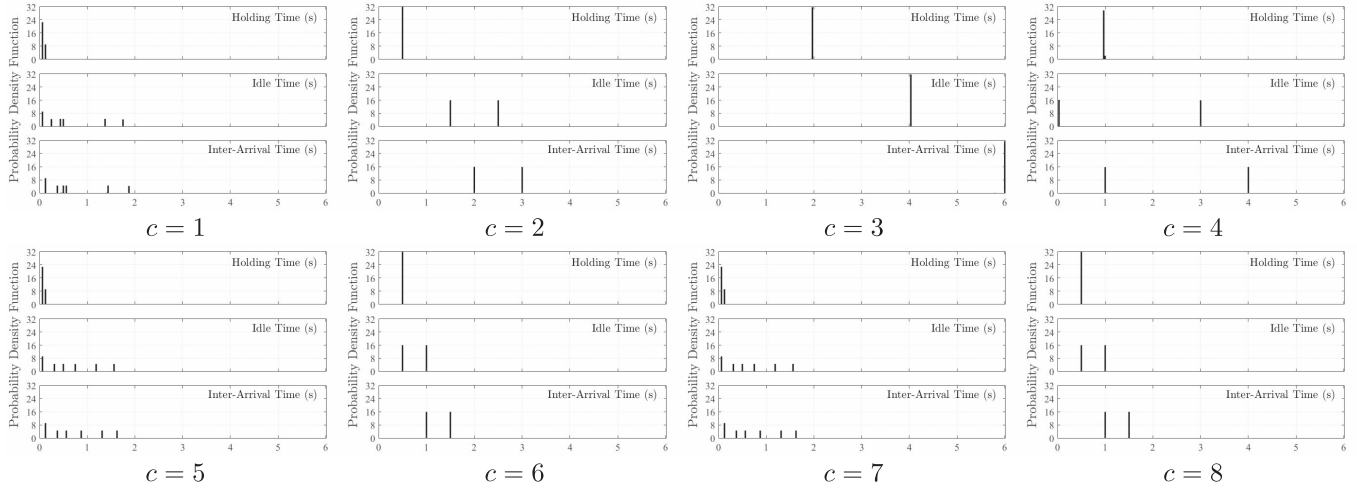


Fig. 4. The experimental holding, idle, and inter-arrival time PDFs over a one-week period, for channel c given in Table I.

#### A. Occupancy Duration Modeling

We can generate the probability density functions (PDF) from this data, over multiple observation periods, to understand the characteristics of each channel. Thus, we produced holding, idle, and inter-arrival time PDFs for every channel over the weekdays, weekend, and the one-week period. However, the PDFs for these were very similar; with slight variations to the height of the bar due to the data size in each grouping. To verify this, the PDFs for each observation period was reviewed per channel which confirmed the results. Furthermore, the signal strength in c=2 partially fell below  $\eta$  during observation periods 15:00 and 18:00 which resulted in missed detections; many significant clusters were formed that could not be corrected in the regrouping stage due to the temporal spacing of the clusters. To address this, a dynamic threshold and a larger  $\varepsilon$  value could be applied to c=2 for improved results but is unnecessary here given the other consistent PDFs. Therefore, we omit the data from observation periods 15:00 and 18:00 for c = 2 and only showcase in Fig. 4 the PDFs for the one-week period.

The PDFs in Fig 4 were generated using bin widths of 31.25 ms with the first bin width being half this value as negative time has no physical meaning in this context. The reason for such small bin widths is due to the short packet bursts in  $c = \{1, 5, 7\}$  and very short idle times in c = 4. The holding times for  $c = \{2, 3, 4, 6, 8\}$  appear to be static throughout the one-week period while  $c = \{1, 5, 7\}$  have two distinct holding times with the shorter holding time occurring approximately twice as often. Likewise,  $c = \{2, 4, 6, 8\}$  have two distinct idle times that appear to occur equally while c=3 has only one idle time. However,  $c=\{1,5,7\}$ have multiple idle times with the shortest idle time occurring more often. An interesting observation that can be made here is that  $c = \{5,7\}$  and  $c = \{6,8\}$  show nearly identical PDFs with very small differences in the heights of the bars. We can further compare these by evaluating the occupancy rates and Lempel-Ziv complexity (LZC). However, the exact

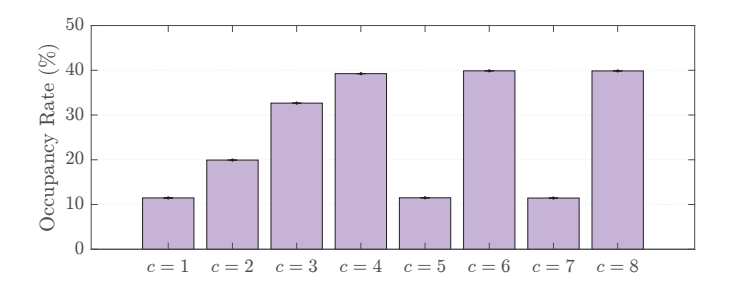


Fig. 5. The mean occupancy rate over a one-week period.

reason for this is unknown, but we can speculate on the potential circumstances that could result in such observations, e.g., the measurement location could be between overlapping satellite beams from the Inmarsat GEO satellite. To verify this, we took brief measurements in Melbourne and Sydney simultaneously and noticed that  $c = \{7, 8\}$  was absent from both captures. However, retaking measurements at the original measurement location still showed  $c = \{7, 8\}$ .

## B. Occupancy Rate Modeling

The spectral occupancy rate provides useful information on the average utilization of the spectrum in time over a fixed period. The occupancy rate can be calculated by

$$R(c) = \frac{\sum_{p=1}^{N_p} T_{H,p}}{T_p} \times 100 \tag{9}$$

where R(c) is the occupancy rate (as a percentage) of channel c and  $T_p$  is the observation recording time integer in seconds. The mean spectrum occupancy results are shown in Fig. 5 for every channel with the standard deviation bars provided. We can see that all the channel occupancies are fixed over time.

We can extend this by calculating and comparing the LZC against the channel occupancy rate. The LZC shows the uncertainty or randomness in time series data and is used here to measure the burstiness of the channel occupancy over time, with the calculation of LZC detailed in [12]. We can obtain a

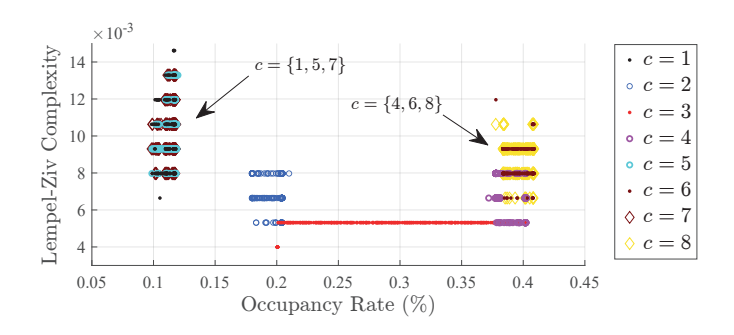


Fig. 6. The duty cycle compared to the channel's burstiness for a random observation period.

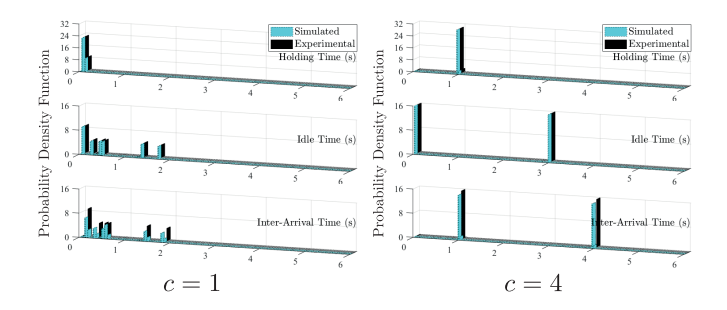


Fig. 7. Comparison between the experimental and simulated PDFs.

binary sequence, that represents the spectrum usage, from  $\mathbf{T}_c$  by converting every  $\{T_{\mathrm{H},p},T_{\mathrm{I},p}\}$  pair to a sequential series of 1's (busy) and 0's (idle) using  $\Delta t$ . The binary sequence for channel c is then divided into sub-sequences of length 10000, which the LZCs and channel occupancy rates are calculated from. The results of this process are given in Fig. 6 for every channel. The channels with similar patterns cluster together, showing overlapping LZC-occupancy rate values. The overlap indicates that the channels have similar traffic behaviors, e.g., Fig. 6 reveals the same aforementioned observation where  $c=\{5,7\}$  and  $c=\{6,8\}$  show nearly identical patterns.

# VI. TRAFFIC MODEL SIMULATION

Simulating a SATCOM system is important to create practical research outcomes, applicable to CR, DSA, and machine learning. A method to simulating one of the SATCOM channels here is by generating a series of  $\{T_H, T_I\}$  pairs for a desired  $N_p$  or time interval. We can generate these values by using the inverse cumulative density function (CDF) sampling method. We simulate  $N_p = 1.5 \cdot 10^6$  packets for channels  $c = \{1, 4\}$  using their experimental discrete PDFs. The time values chosen for simulating  $T_{\rm H}$  and  $T_{\rm I}$  were the center values of the PDF bins, i.e., discrete time values of  $\{15.625, 31.2562.5, 93.75, 125, ...\}$  ms. Let  $T_0 = 0$  track the start time of the packets. Until all packets have been processed, the random values were generated uniformly and mapped to the CDF to find the  $T_{\mathrm{H},p}$  and  $T_{\mathrm{I},p}$  center bin values. The simulated packet is constructed by  $T_{s,p} = T_0$ and  $T_{e,p} = T_0 + T_{H,p}$  where  $1 \le p \le N_p$ . Lastly, the value of  $T_0$  is increased by  $T_{\rm H}+T_{\rm I}$ . The experimental and simulated PDFs are presented in Fig. 7 which are almost identical. The simulated inter-arrival times in c=1 do not match the experimental results because the observed traffic does not use back-to-back 'long' bursts. To extend this work, synthetic I/Q satellite traffic can be generated from these simulated  $T_{\rm H}$  and  $T_{\rm I}$  values, which could have varying power levels, to be applied to CR, DSA, and machine learning.

# VII. CONCLUSION

This paper presented a framework for experimental satellite channel spectrum occupancy measurements and modeling. We developed an inexpensive testbed to capture satellite-to-earth signals in the L-band and detailed the processing steps to extract the occupancy information from the captured data using a combination of time-frequency and clustering algorithms. The experimental PDFs were created which showed the occupancy duration of the traffic and we obtained the occupancy rate using the *packets* in the satellite channels. We generated the holding and idle times for several satellite channels using the experimental PDFs to simulate a series of satellite *packets*. The results from this paper helps researchers to develop CR- and DSA-based SATCOM systems to better utilize the spectrum with improved efficiency.

## ACKNOWLEDGMENT

This work has been supported by the SmartSat CRC, whose activities are funded by the Australian Government's CRC Program.

# REFERENCES

- FCC. (2024) 2024 Communications Marketplace Report. [Online].
   Available: https://docs.fcc.gov/public/attachments/FCC-24-136A1.pdf
- [2] Inmarsat. (2023) Space Explained. [Online]. Available: https://www.inmarsat.com/en/insights/corporate/2023/what-issatellite-spectrum-used-for.html
- [3] ITU. (2023) Visions for space services at the World Radiocommunication Conference. [Online]. Available: https://www.itu.int/en/itunews/Documents/2023/2023-04/2023\_ITUNews04-en.pdf
- [4] —... (2011) Spectrum Monitoring Handbook. [Online]. Available: https://www.itu.int/dms\_pub/itu-r/opb/hdb/R-HDB-23-2011-PDF-E.pdf
- [5] K. Patil, K. Skouby, A. Chandra, and R. Prasad, "Spectrum occupancy statistics in the context of cognitive radio," in 2011 The 14th International Symposium on WPMC, 2011, pp. 1–5.
- [6] A. Marţian, A. Achim, O. Fratu, and I. Marghescu, "Analysis of frequency spectrum usage from a cognitive radio perspective," in 2010 3rd ISABEL, 2010, pp. 1–5.
- [7] R. I. C. Chiang, G. B. Rowe, and K. W. Sowerby, "A Quantitative Analysis of Spectral Occupancy Measurements for Cognitive Radio," in 2007 IEEE 65th VTC (Spring), 2007, pp. 3016–3020.
- [8] B. A. Homssi, A. Al-Hourani, Z. Krusevac, and W. S. T. Rowe, "Machine learning framework for sensing and modeling interference in iot frequency bands," *IEEE IoT Journal*, vol. 8, no. 6, pp. 4461– 4471, 2021.
- [9] SDRplay. (2020) RSPduo Dual Tuner 14-bit SDR Datasheet. [Online].Available: https://www.sdrplay.com/docs/RSPduoDatasheetV0.5.pdf
- [10] —. (2018) RSPduo Technical Specifications. [Online]. Available: https://www.sdrplay.com/wp-content/uploads/2018/06/RSPDuo-Technical-Information-R1P1.pdf
- [11] M. Aygur, S. Kandeepan, A. Al-Hourani, E. Arbon, and Z. Kursevac, "Spectrum Sensing Using Semantic Segmentation for Hybrid Satellite-Terrestrial Applications," in 2025 IWCMC, 2025, pp. 1318–1323.
- [12] A. Lempel and J. Ziv, "On the Complexity of Finite Sequences," *IEEE Transactions on Information Theory*, vol. 22, no. 1, pp. 75–81, 1976.